A&A 632, A25 (2019)
https://doi.org/10.1051/0004-6361/201936764

Astronomy & Astrophysics

VLT/SPHERE exploration of the young multiplanetary system PDS70[⋆,⋆⋆]

D. Mesa[1], M. Keppler[2], F. Cantalloube[2], L. Rodet[3], B. Charnay[4], R. Gratton[1], M. Langlois[5,6], A. Boccaletti[4], M. Bonnefoy[3], A. Vigan[6], O. Flasseur[7], J. Bae[8], M. Benisty[3,9], G. Chauvin[3,9], J. de Boer[10], S. Desidera[1], T. Henning[2], A.-M. Lagrange[3], M. Meyer[11], J. Milli[12], A. Müller[2], B. Pairet[13], A. Zurlo[14,15,6], S. Antoniucci[16], J.-L. Baudino[17], S. Brown Sevilla[2], E. Cascone[18], A. Cheetham[19], R. U. Claudi[1], P. Delorme[3], V. D'Orazi[1], M. Feldt[2], J. Hagelberg[19], M. Janson[20], Q. Kral[4], E. Lagadec[21], C. Lazzoni[1], R. Ligi[22], A.-L. Maire[2,23], P. Martinez[21], F. Menard[3], N. Meunier[3], C. Perrot[4,24,25], S. Petrus[3], C. Pinte[26,3], E. L. Rickman[19], S. Rochat[3], D. Rouan[4], M. Samland[2,20], J.-F. Sauvage[27,6], T. Schmidt[4,28], S. Udry[19], L. Weber[19], and F. Wildi[19]

(Affiliations can be found after the references)

Received 23 September 2019 / Accepted 24 October 2019

ABSTRACT

Context. PDS 70 is a young (5.4 Myr), nearby (~113 pc) star hosting a known transition disk with a large gap. Recent observations with SPHERE and NACO in the near-infrared (NIR) allowed us to detect a planetary mass companion, PDS 70 b, within the disk cavity. Moreover, observations in H_α with MagAO and MUSE revealed emission associated to PDS 70 b and to another new companion candidate, PDS 70 c, at a larger separation from the star. PDS 70 is the only multiple planetary system at its formation stage detected so far through direct imaging.

Aims. Our aim is to confirm the discovery of the second planet PDS 70 c using SPHERE at VLT, to further characterize its physical properties, and search for additional point sources in this young planetary system.

Methods. We re-analyzed archival SPHERE NIR observations and obtained new data in Y, J, H and K spectral bands for a total of four different epochs. The data were reduced using the data reduction and handling pipeline and the SPHERE data center. We then applied custom routines (e.g., ANDROMEDA and PACO) to subtract the starlight.

Results. We re-detect both PDS 70 b and c and confirm that PDS 70 c is gravitationally bound to the star. We estimate this second planet to be less massive than 5 $M_{\rm Jup}$ and with a $T_{\rm eff}$ around 900 K. Also, it has a low gravity with $\log g$ between 3.0 and 3.5 dex. In addition, a third object has been identified at short separation (~0.12″) from the star and gravitationally bound to the star. Its spectrum is however very blue, meaning that we are probably seeing stellar light reflected by dust and our analysis seems to demonstrate that it is a feature of the inner disk. We cannot however completely exclude the possibility that it is a planetary mass object enshrouded by a dust envelope. In this latter case, its mass should be of the order of a few tens of $M_\oplus$. Moreover, we propose a possible structure for the planetary system based on our data, and find that this structure cannot be stable on a long timescale.

Key words. instrumentation: spectrographs – methods: data analysis – techniques: imaging spectroscopy – planetary systems – stars: individual: PDS70

1. Introduction

PDS 70 is a K7 pre-main sequence star of 5.4 ± 1.0 Myr in age (Müller et al. 2018) that is part of the Upper Centaurus-Lupus group (Pecaut & Mamajek 2016) at a distance of 113.43 ± 0.52 pc (Gaia Collaboration 2016, 2018). In the course of the VLT/SPHERE SHINE survey (Chauvin et al. 2017), Keppler et al. (2018) discovered a planetary mass companion, PDS 70 b, located in the transition disk surrounding this young star. The presence of a circumstellar disk was first inferred by Metchev et al. (2004) due to the detection of a strong mid-infrared (MIR) excess and of a strong emission at millimeter wavelengths. The disk was first resolved in K_s band by Riaud et al. (2006) using VLT/NACO. The first detection of a gap in the disk was obtained by Hashimoto et al. (2012) exploiting H-band polarized data obtained through the Subaru/HiCIAO instrument. Using the same data, Dong et al. (2012) estimated, assuming a distance of 140 pc for the system, a gap size of around 65 au in which the dust is depleted by a factor of approximately 1000 with respect to the outer part of the disk. These latter authors also found evidence of an inner disk with dimensions of the order of few astronomical units detecting a weak near-infrared (NIR) excess in the spectral energy distribution (SED); they estimated a total dust mass of $\sim 10^{-4}$ $M_\odot$ for the disk. PDS 70 was also observed at millimeter wavelengths by Hashimoto et al. (2015) using the Submillimeter Array (SMA) and, more recently, by Long et al. (2018) using ALMA. The ALMA observations were performed both at 0.87 mm continuum and at HCO^+ and CO gas emission lines. These allowed the presence of a radial gap between the inner and the outer disk at 15–60 au of separation to be defined in the dust continuum, assuming a distance of 140 pc, and different substructures to be imaged, such as a bridge-like feature and an azimuthal gap in the HCO^+ emission

⋆ The reduced images are also available at the CDS via anonymous ftp to cdsarc.u-strasbg.fr (130.79.128.5) or via http://cdsarc.u-strasbg.fr/viz-bin/cat/J/A+A/632/A25

⋆⋆ Based on observation made with European Southern Observatory (ESO) telescopes at Paranal Observatory in Chile, under programs ID 095.C-0298(B), 1100.C-0481(D), 1100.C-0481(L) and 1100.C-0481(M).

of the disk. Further observations with ALMA in the continuum and CO at higher angular resolution were presented by Keppler et al. (2019), showing evidence of a depletion of emission in the CO integrated intensity centered on the separation of PDS 70 b, while the continuum peak is located at 74 au. Moreover, these latter authors used hydrodynamical modelling of the gas kinematics to find that the presence of an additional low-mass companion further out than the orbit of PDS 70 b may be required to account for the large gap width.

PDS 70 b was detected in the disk gap using NICI, NACO, and VLT/SPHERE data in the NIR by Keppler et al. (2018). Its colors are very red and through photometry these authors were able to estimate a mass of the order of 5–9 $M_{\rm Jup}$ assuming the same age as the system for the companion. The outer disk, as seen at NIR wavelengths, has a radius of about 54 au assuming the updated value of 113.43 pc for the system. Moreover, for the first time these latter authors were able to detect scattered light from the inner disk determining a radius of less than 17 au, consistent with ALMA values. Exploiting new SPHERE observations, Müller et al. (2018) performed a characterization of the orbital properties of PDS 70 b constraining its semi-major axis around 22 au corresponding to an orbital period of ~118 yr. Using the planet IR spectrum and atmospheric models, these latter authors found for the companion a $T_{\rm eff}$ between 1000 and 1600 K, low surface gravity (<3.5 dex), and an unusually large radius of between 1.4 and 3.7 $R_{\rm Jup}$. The latter could suggest the presence of circumplanetary material. Recent observations in H and K bands with VLT/SINFONI may indicate the presence of a circumplanetary disk around PDS 70 b to explain its very red spectrum (Christiaens et al. 2019a,b).

Following the PDS 70 b discovery, observations at Hα wavelength with the *Magellan* Adaptive Optics (MagAO) system (Wagner et al. 2018) revealed a source in Hα at the position of the companion. This is a hint that PDS 70 b is still accreting material and is consistent with the presence of a circumplanetary disk. The authors were able to derive a value of $10^{-8\pm1}$ $M_{\rm Jup}$ yr^{-1} for the mass accretion rate. This result was later independently confirmed with VLT/MUSE observations (Haffert et al. 2019) where the authors redetected PDS 70 b in $H\alpha$ and derived an accretion rate of $2\times10^{-8\pm0.4}$ $M_{\rm Jup}$ yr^{-1}. A new clear point-source emission was detected with a signal-to-noise ratio (S/N) of around 8 at larger separation (~35 au) very near to the bright west ring of the disk as seen in projection, suggesting the presence of a second companion in the PDS 70 system (hereinafter PDS 70 c). The authors were able to estimate an accretion rate of $10^{-8\pm0.4}$ $M_{\rm Jup}$ yr^{-1} for this object. The reanalyis of the ALMA data previously used by Long et al. (2018) and by Keppler et al. (2019) allowed Isella et al. (2019) to detect a submillimeter continuum emission associated with PDS 70 c interpreted as originating from a dusty circumplanetary disk. These latter authors also detected a second compact source at close separation from PDS 70 b speculating that this could come from dust orbiting in the proximity of the planet.

The direct imaging signal of PDS 70 c was marginally identified in SPHERE NIR data in the form of a rather elongated structure but not presented in Keppler et al. (2018) and Müller et al. (2018) because of possible contamination from the disk. Further SPHERE follow-up observations were performed with the aim being to provide a robust independent confirmation of the existence of PDS 70 c, to further characterize its nature, and finally to search for additional point-sources in the system.

In this paper, we present in Sect. 2 the data that we use for our analysis and the data reduction procedure. In Sect. 3 we present our results while in Sect. 4 we discuss them. Finally, in Sect. 5 we give our conclusions.

2. Observations and data reduction

For the present work we used both archival and new observations taken with SPHERE (Beuzit et al. 2019). The archival observations were obtained on the nights of 2015-05-31 and 2018-02-24 and were previously used for the works presented in Keppler et al. (2018) and in Müller et al. (2018). In addition to these data we also acquired new data on the nights of 2019-03-06 and 2019-04-13. The main characteristics of all these observations are presented in Table 1. The first of these observations was carried out in the IRDIFS mode, that is with IFS (Claudi et al. 2008) operating in Y and J spectral bands (between 0.95 and 1.35 μm) and IRDIS (Dohlen et al. 2008) operating in the H band with the H23 filter pair (wavelength H2 = 1.593 μm; wavelength H3 = 1.667 μm; Vigan et al. 2010). The remaining observations were performed using the IRDIFS_EXT mode that uses IFS in Y, J, and H spectral band (between 0.95 and 1.65 μm) and IRDIS exploiting the K band with the K12 filter pair (K1 = 2.110 μm and K2 = 2.251 μm). Due to technical problems, the star was offset by ~20 mas in the southeast direction with respect to the coronagraphic mask during the 2019-03-06 observations. On the last observing date we used a coronagraph that was not optimized for the IRDIFS_EXT mode but that had a smaller inner working angle, with a diameter of 145 mas, allowing us to observe possible objects at small separations from the central star. This, however, did not allow us to obtain good astrometric and photometric measurements for PDS 70 b and PDS 70 c and for this reason we were not able to use these values for this epoch in the following work. At all the epochs, we obtained frames with satellite spots symmetric with respect to the central star before and after the coronagraphic sequences. This enabled us to determine the position of the star behind the coronagraphic focal plane mask and accurately recenter the data. Furthermore, to be able to correctly calibrate the flux of companions, we acquired images with the star off-axis. In these cases, the use of an appropriate neutral density filter was mandatory to avoid saturation of the detector.

The data were reduced through the SPHERE data center (Delorme et al. 2017) applying the appropriate calibrations following the data reduction and handling (DRH; Pavlov et al. 2008) pipeline. In the IRDIS case, the requested calibrations are the dark and flat-field correction and the definition of the star center. In addition to the dark and flat-field corrections, IFS requires the definition of the position of each spectra on the detector, the wavelength calibration, and the application of the instrumental flat field. On the pre-reduced data we then applied speckle-subtraction algorithms like TLOCI (Marois et al. 2014) and a principal components analysis (PCA; Soummer et al. 2012) as implemented in the consortium pipeline application called SpeCal (Spectral Calibration; Galicher et al. 2018) and also described in Zurlo et al. (2014) and in Mesa et al. (2015) for the IFS. Finally, the ANDROMEDA package (Cantalloube et al. 2015) and the PACO package (Flasseur et al. 2018) were also applied to all datasets.

3. Results

The final images obtained using PCA are shown in Fig. 1 both for IFS (upper panels) and IRDIS (bottom panels). PDS 70 b is visible in all these images but in the following we focus on the detection of other point sources.

Table 1. Main characteristics of the SPHERE observations of PDS 70 used for this work.

Date	Obs. mode	Coronograph	DIMM seeing	τ_0	Wind speed	Field rotation	DIT	Total exposure
2015-05-31	IRDIFS	N_ALC_YJH_S	1.20″	1.1 ms	4.55 m s^{-1}	50.6°	64 s	4096 s
2018-02-24	IRDIFS_EXT	N_ALC_YJH_S	0.40″	7.0 ms	2.85 m s^{-1}	93.4°	96 s	6336 s
2019-03-06	IRDIFS_EXT	N_ALC_K_s	0.39″	8.9 ms	4.45 m s^{-1}	56.5°	96 s	4608 s
2019-04-13	IRDIFS_EXT	N_ALC_YJ_S	0.98″	2.5 ms	8.53 m s^{-1}	71.4°	96 s	6144 s

Notes. During the observation of 2019-03-06, the coronagraph was incorrectly positioned with an offset of ∼20 mas in the southeast direction.

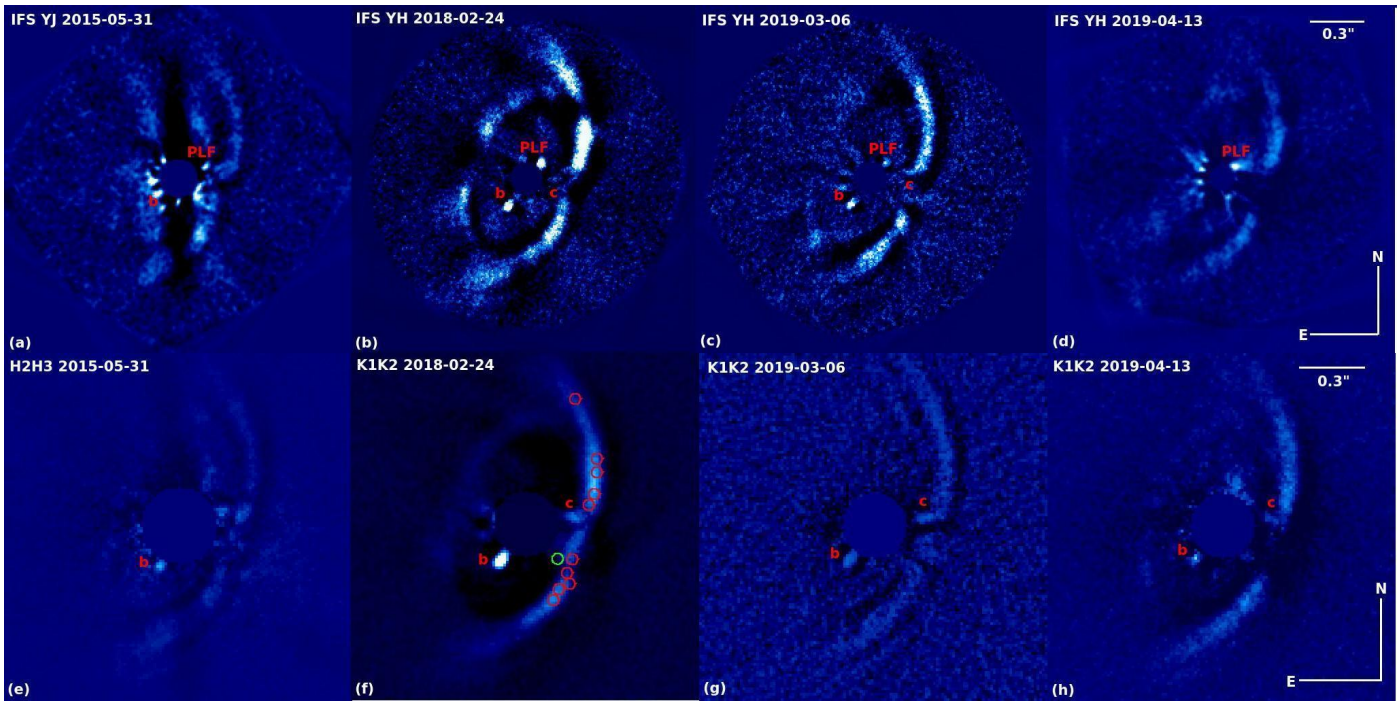

Fig. 1. Final IFS (*upper row*) and IRDIS (*bottom row*) images obtained for the following epochs: 2015-05-31 (*panels a* and *e*), 2018-02-24 (*panels b* and *f*), 2019-03-06 (*panels c* and *g*) and 2019-04-13 (*panels d* and *h*). The scale and the orientation are the same for all the epochs and are displayed in *panels d* and *h*. In each image we tag with red letters the positions of the identified companions and of the proposed PLF. All the images displayed have been obtained using a PCA of five principal components applied separately on each wavelength apart from for the first IFS image where just two principal components were used. In *panel f* we overplot ten red circles to indicate the positions used to extract the disk spectra and one green circle for the position of the simulated planet as described in more detail in Sect. 4.1.

The re-analysis of these images allowed us to detect PDS 70 c at S/Ns of 8.6 and 9.6 at a projected separation of ∼0.2″ in the IRDIS data acquired during the nights of 2018-02-24 and 2019-03-06 (panels f and g of Fig. 1), respectively. PDS 70 c is visible at the same epochs in the IFS images (panels b and c of Fig. 1) and is barely visible in the IRDIS image obtained from 2019-04-13 data (panel h of Fig. 1).

A third object is clearly visible at short separation from the star both in the 2018-02-24 and in the 2019-03-06 IFS data (panels b and c of Fig. 1) with a S/N of ∼5. As we discuss in the following sections, even if the planetary nature of this object cannot be fully excluded, our analysis favors a scenario where this object is an inner disk feature. For this reason we hereinafter refer to this detection as a point-like feature (PLF). The source was also retrieved in the IFS 2019-04-13 observation (panel d of Fig. 1), during which we used a setup optimized to retrieve objects at very close separation from the star, as explained above. Furthermore, we were able to find the same object at very low S/N in an older observation (2015-05-31, see panel a of Fig. 1). This allowed us to expand the time range of our observations. For the IRDIS data, this object can only be barely retrieved in the 2018-02-24 data while it is not visible in the remaining epochs. However, given the poor detection, the photometry could not be extracted from these data using either the negative planet method or the ANDROMEDA package. It was however possible to retrieve photometry using the PACO package.

We then combined the images at different epochs to obtain a complete vision of the PDS 70 planetary system and to determine in a more precise way its structure following the method described in Gratton et al. (2019). We used the IFS images because it was possible to clearly image all of the proposed companions around the star. As a first step we deprojected our data, assuming a disk inclination and a position angle of 49.7° and 158.6° respectively (Hashimoto et al. 2012; Keppler et al. 2019), to be able to see the disk plane face-on. We then rotated the images according to circular Keplerian motion to have the three objects in the same positions at different epochs and sum the images. Given the short total orbital rotation of the companions in the considered time range, the effects of the uncertainties on the stellar and companion masses are not relevant in the final result of this procedure. Finally, we projected back our data to obtain a view of the system as seen on-sky.

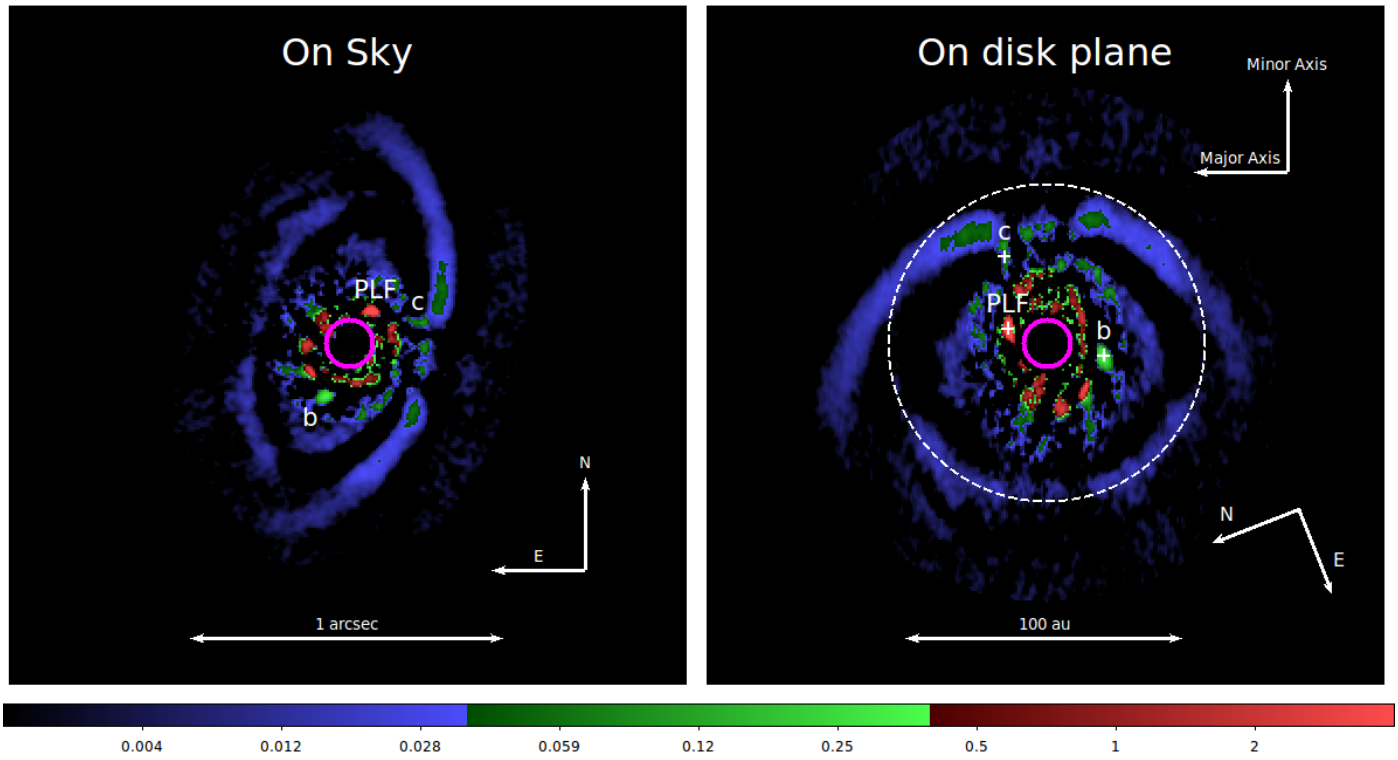

Fig. 2. *Left*: IFS image obtained combining the images from all the epochs as described in the text. The positions of the three objects known around PDS 70 are tagged. *Right*: deprojected image of the PDS 70 system as seen on the disk plane. The dashed circle indicates the position of the inner edge of the outer ring of the disk as found with ALMA by Keppler et al. (2019) to show that it corresponds to the partially imaged ring in the SPHERE images.

The final result of this procedure is shown in Fig. 2 where the left panel shows the on-sky view of the system with the indication of the positions of the three proposed objects. On the right panel, we instead show the deprojected view of the system seen in the disk plane. Furthermore, we note that the position of the western outer ring of the disk, apparently very near to the position of PDS 70 c, is due to a projection effect, because the bright western part of the disk seen in scattered light is actually the upper layer of a torus at a certain height with respect to the disk plane. This is similar to other cases observed with SPHERE, like for example RX J1615.3-3255 (de Boer et al. 2016) and HD 100546 (Sissa et al. 2018).

A complete discussion of the structure of the disk is however beyond the scope of this paper, which is focused on the confirmation and characterization of PDS 70 c and on the additional point-like feature in this system.

3.1. PDS 70 b

The new SPHERE data did not allow us to update the spectral results given in Müller et al. (2018) for PDS 70 b. We therefore refer to this paper for any information about the spectral analysis for this object. We used our recent SPHERE data to update the orbital solutions of PDS 70 b which are in good agreement with what was found by Müller et al. (2018). The results of this analysis are given in the top right panel of Fig. 3, in Sects. 3.4 and 4.3.

3.2. PDS 70 c

The main limitation to the analysis of this object with SPHERE is that it is projected very near to the bright western ring of the disk. This prevented a robust identification in previous analyses as it was regarded as a feature of the disk and, moreover, complicated both the astrometric and photometric extraction. In our new analysis, we were able to obtain these values using the negative planet method (see e.g., Bonnefoy et al. 2011; Zurlo et al. 2014) for the two best observing epochs (2018-02-24 and 2019-03-06) and confirm that it is actually a planet. In Table 2 we list the astrometric values obtained from the IRDIS data for the two available epochs through this approach. The relative positions of PDS 70 c are also shown in the bottom left panel of Fig. 3 where they are compared to the positions expected for a background object. This allows us to exclude that this is a background object.

The negative planet method was also used to calculate the photometric values. However, due to the faintness of this object in the Y, J, and H spectral bands, we had to perform this method using the average over five consecutive spectral channels. This meant that we could not derive any photometric value for the first two and the last two IFS channels. The final spectrum is obtained through a weighted average, with the weight considering the different qualities of the observations, of the results obtained for the last three epochs considered here. To check the reliability of this result we extracted the spectrum also using the ANDROMEDA and the PACO package. ANDROMEDA gave results comparable to those from the first method as shown in Fig. 4, apart from the fact that the negative planet method gives negative values in the spectral region around 1.4 μm. These values are likely related to water telluric absorption affecting both the stellar and the planet flux but we cannot exclude that they are linked to the effect of the data-reduction method. The same feature is not present in the ANDROMEDA spectrum. On the other hand, the spectrum extracted with PACO had a detection limit below 3σ and so we did not consider it as a reliable detection and do not use it for this

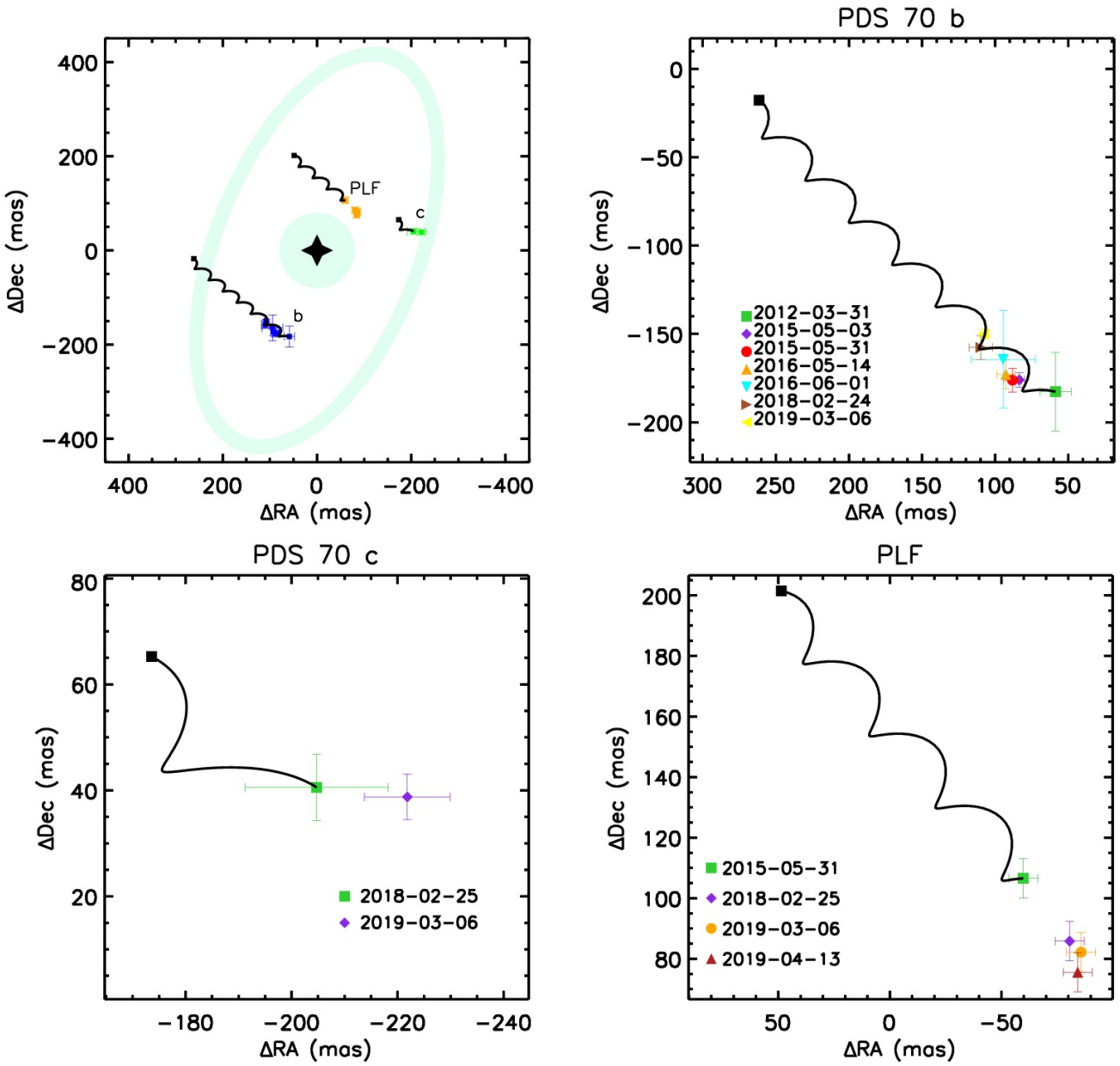

Fig. 3. *Top left panel*: relative astrometric positions of the three proposed companions of PDS 70 with respect to the host star, represented by the black star symbol. The positions of the inner and of the outer disk are also displayed through light cyan areas. The solid black lines represent the expected course of the companion if it were a background object. The length differences between the black lines for different objects are due to the different temporal coverage that we have for each of them. The black squares at the end of the line represent the expected position at the epoch of the last observation in this case. For clarity, we show a zoomed-in version of the areas around each companion in the *top right panel* for PDS 70 b, in the *bottom left panel* for PDS 70 c, and in the *bottom right panel* for the PLF.

Table 2. Astrometric and photometric (absolute magnitudes) results obtained for PDS 70 c.

Date	ΔRA (″)	ΔDec (″)	ρ (″)	PA	M_J	M_H	M_{K1}	M_{K2}
2018-02-24	-0.205 ± 0.013	0.041 ± 0.006	0.209 ± 0.013	281.2 ± 0.5	17.45 ± 0.33	14.89 ± 0.87	12.69 ± 0.17	12.53 ± 0.19
2019-03-06	-0.222 ± 0.008	0.039 ± 0.004	0.225 ± 0.008	279.9 ± 0.5	17.00 ± 0.40	14.90 ± 0.90	12.49 ± 0.11	12.25 ± 0.14

work. Instead, its results for the IRDIS data are in good agreement with those for ANDROMEDA as shown in Fig. 4. For all the reason listed above, we therefore use only the results from the ANDROMEDA package in the following analysis. The result of this procedure is displayed in panel a of Fig. 5 where the green squares are the photometric values obtained from IFS while the violet squares are obtained from IRDIS. The extracted spectrum displays very red colors providing further confirmation of the planetary nature of this object as also confirmed by comparing it to the solid cyan line that represents the extracted spectrum for a speckle from the same dataset, obtained before applying the speckle-subtraction procedure at a separation comparable to

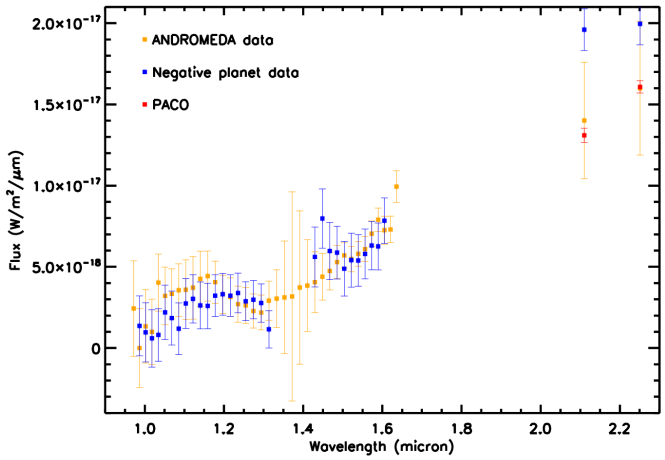

Fig. 4. Comparison between the PDS 70 c spectrum extracted using the negative planet method (blue squares), ANDROMEDA (orange squares), and PACO (magenta squares). For the latter method, we plot only the two values obtained from IRDIS data. As in the region around 1.4 μm the negative planet method gives negative values, those points are not shown in the plot.

that of the companion. Using these results we can also derive the photometric results in different spectral bands that are listed for the two epochs in which it is visible in Table 2.

3.3. PLF

Like for the case of PDS 70 c we extracted astrometric and photometric values for the PLF following the same methods. In this case however, we were able to obtain the astrometric values in all four observing epochs exploited for this work using only the IFS data. This supports the fact that the signal is not an artefact from the data processing. The astrometric values for this object are listed in Table 3 while its relative positions are compared to those expected for a background object in the bottom right panel of Fig. 3. Also in this case, the analysis confirms that this source is gravitationally bound to PDS 70. As done for PDS 70 c, the spectrum extraction was performed using the negative planet procedure, the ANDROMEDA package, and the PACO package, leading to comparable results for the IFS data. Due to the fact that it was possible to detect this object only marginally in IRDIS data, it was not possible to extract any reliable photometry with the first two methods while this was possible using the PACO package. We then used these values for the spectrum of this object, which is shown in panel b of Fig. 5. PACO could lead to an underestimation of the error bars with respect to other methods due to a difference in the way it calculates them, as can be seen in Fig. 5. While this can lead to some inconsistency, we included its results to give a more complete view of the characteristics of this object. The PLF appears blue and very similar to the stellar spectrum at these wavelengths as demonstrated by the blue solid line plotted in the same figure obtained using a calibrated spectrum of PDS 70 from the SpeX spectrograph following Müller et al. (2018). To be able to overplot the two spectra, we normalized the stellar spectrum to the flux of the companion. This is a strong hint that the PLF spectrum is probably mainly due to the reflection of the stellar light from dust.

3.4. Structure of the PDS 70 planetary system

To constrain the fundamental orbital parameters for the three candidate companions, we ran a Monte-Carlo simulation using the Thiele-Innes formalism (Binnendijk 1960) as devised in Desidera et al. (2011), and Zurlo et al. (2013, 2018) and adopting the convention of Heintz (2000). The simulation generates 5×10^7 orbits and rejects all those that do not fit the astrometric data. With this aim, we assumed for the star a mass of 0.76 $M_\odot$ and a distance of 113.43 pc. Moreover, we assumed a circular orbit for each companion. In this way, for PDS 70 b we found an orbital radius of $22.7^{+2.0}_{-0.5}$ au, a period of $123.5^{+9.8}_{-4.9}$ yr, and an orbit inclination of $39.7^{+5.4}_{-2.8}$ degrees, in good agreement with what was found by Müller et al. (2018). Due to the paucity of astrometric points, the results for PDS 70 c are less defined than for PDS 70 b; we obtained a radius of $30.2^{+2.0}_{-2.4}$ au, a period of $191.5^{+15.8}_{-31.5}$ yr, and an inclination of $40.8^{+30.3}_{-14.0}$ degrees. Finally, for the PLF orbit we obtained a radius of $13.5^{+0.3}_{-0.2}$ au, a period of $56.3^{+2.0}_{-1.1}$ yr, and an inclination of $46.5^{+2.3}_{-10.4}$ degrees.

We combined these results with those for the disk (Keppler et al. 2019) to generate a model for the structure of the planetary system around PDS 70. The values of the estimated separation expressed in astronomical units both for the companion and for the part of the disk, together with the Keplerian rotation period, the companion masses as calculated in Sects. 4.1 and 4.2 and the ratio between the object period and the period of PDS 70 b are listed in Table 4. From these data we can see that, if the PLF is a planet, its orbit is in 2:1 resonance with the outer edge of the inner disk while a 3:2 resonance can be found between the orbits of PDS 70 b and PDS 70 c.

4. Discussion

4.1. The nature of PDS 70 c

The projected position of PDS 70 c is very close to the bright west part of the disk. This raises the concern that the spectrum shown in the panel a of Fig. 5 could be contaminated and therefore biased by the disk signal. To examine this possibility we extracted the spectrum of the disk (using both IFS and IRDIS photometry) at ten different positions of the disk as indicated by the red circles in panel f of Fig. 1. Due to the fact that we are extracting the photometry of an extended structure, it is not possible to use the negative planet procedure as we did for PDS 70 c. We then applied an aperture photometry method, using an aperture with a radius of three pixels. We then made a median of these spectra to compare the resulting spectrum with that extracted for the companion. The result of this procedure is displayed in panel c of Fig. 5 where the spectra of the companion and of the disk are represented by the green and the brown squares, respectively. We can see that while at short wavelengths the two spectra are very similar, they diverge starting from the IFS H-band and are very different in the IRDIS K-band. As a further test to see whether or not the disk can influence the companion spectrum extraction, we injected into our datacube a simulated planet in a position similar to PDS 70 c with respect to the disk. The position of the simulated companion is indicated by a green circle in panel f of Fig. 1. The input spectrum of the simulated planet was obtained scaling the spectrum of PDS 70 b. After that, we extracted the companion spectrum using the same method as used for PDS 70 c. The result of this procedure is displayed in panel d of Fig. 5 where the input spectrum is represented by the blue line while the orange squares are the extracted photometric values. From these results we can conclude that we are able to faithfully reproduce the input spectrum of the simulated planet. Given the similarity of this case with that of PDS 70 c, we conclude that the results of these tests support the hypothesis that the signal comes from a point-like source not

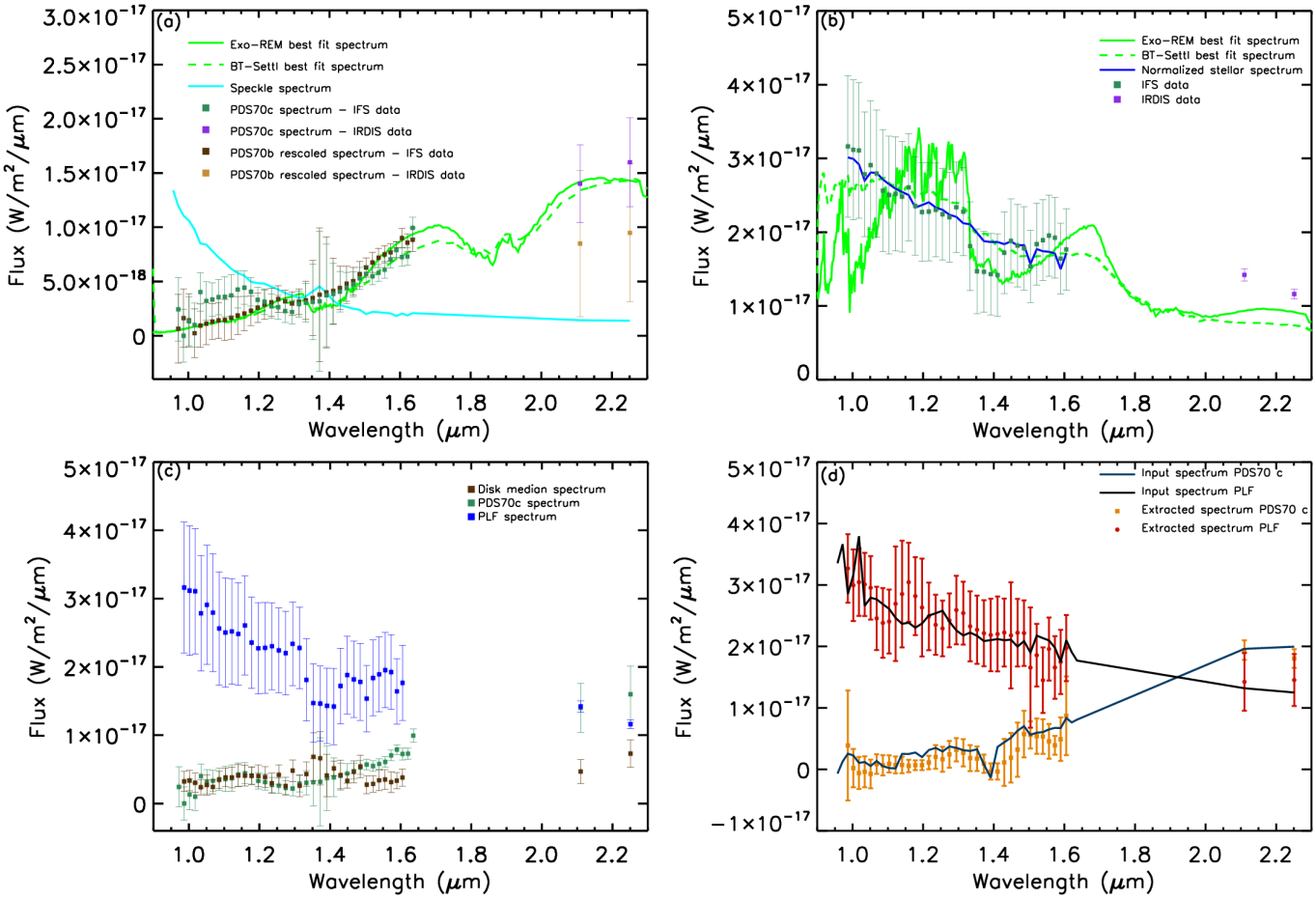

Fig. 5. *Panel a*: extracted spectrum of PDS 70 c both with IFS (green squares) and IRDIS (violet squares). The green solid line represents the best fit Exo-REM model while the green dashed line is the best fit BT-Settl model. The parameters of the best-fit models are listed in the text (Sect. 4.1). The cyan solid line represents an extracted spectrum for a speckle from the same dataset. We also overplot the rescaled spectrum of PDS 70 b both for IFS (deep brown squares) and IRDIS (light brown squares). *Panel b*: same as panel a but for the PLF spectrum. We plot as a blue solid line the stellar spectrum normalized to the companion flux to demonstrate their similarity. *Panel c*: comparison between the extracted spectra for PDS 70 c and the PLF and the spectrum obtained making a median of ten different positions of the disk. *Panel d*: comparison between the injected spectrum of a simulated planet in a position similar to PDS 70 c with respect to the disk (deep blue solid line) and the relative extracted spectrum (orange squares). The same thing is done for a simulated planet at a similar position of the PLF (black solid line and red circles).

Table 3. Astrometric results obtained for the PLF.

Date	ΔRA (″)	ΔDec (″)	ρ (″)	PA
2015-05-31	-0.060 ± 0.007	0.107 ± 0.007	0.122 ± 0.007	330.7 ± 0.5
2018-02-24	-0.081 ± 0.004	0.086 ± 0.004	0.118 ± 0.004	316.8 ± 0.5
2019-03-06	-0.086 ± 0.004	0.082 ± 0.004	0.119 ± 0.004	313.8 ± 0.5
2019-04-13	-0.084 ± 0.004	0.076 ± 0.004	0.113 ± 0.004	311.7 ± 0.5

related to the circumstellar disk and is of planetary origin. However, it is important to stress that in the Y- and J-spectral bands, the signals from the companion and from the disk are both very low and virtually indistinguishable, meaning that while we use them to define the physical characteristics of the companion, the final results should be regarded with caution, and only provide upper limits.

Moreover, we can check the reliability of the extracted spectrum by comparing it to the spectrum of PDS 70 b. In panel a of Fig. 5 we overplot the extracted spectrum for PDS 70 b, rescaled to be able to compare it with that of PDS 70 c. For this purpose, we used a calculated rescaling factor of 0.18. The two spectra are very similar indicating that both these objects possess red and dusty atmospheres and/or circumplanetary disks.

We estimated the mass of PDS 70 c by comparing the photometric values reported in Table 2 with the AMES-DUSTY models (Allard et al. 2001) assuming a system age of 5.4 ± 1.0 Myr. The error bars on the age could be underestimated for late-type Scorpius-Centaurus stars due to the fact that the effects of the magnetic activity are not taken properly into account as found by Asensio-Torres et al. (2019) for the case of HIP 79124. The results of this procedure are listed in Table 5. The error bars are obtained taking into account the uncertainties on the distance of the system, those on the age of the system, and those on the extracted photometry. The mass values estimated are in good agreement between the different wavelength bands and point toward a planetary object with a mass just above 4 $M_{\rm Jup}$. We notice here that these determinations assume that the observed

Table 4. Structure of the PDS 70 planetary system.

Object	Mass ($M_{\rm Jup}$)	Separation (au)	Period (yr)	$P_{\rm obj}/P_{\rm PDS\,70\,b}$
Inner disk	//	9.1	31.5	0.26
PLF	0.05–0.28	$13.5^{+0.3}_{-0.2}$	$56.3^{+2.0}_{-1.1}$	0.46
PDS 70 b	5.0–9.0	$22.7^{+2.0}_{-0.5}$	$123.5^{+9.8}_{-4.9}$	1.00
PDS 70 c	4.4 ± 1.1	$30.2^{+2.0}_{-2.4}$	$191.5^{+15.8}_{-31.5}$	1.55
Outer disk (ring 1)	//	60.0	533.1	4.32
Outer disk (ring 2)	//	74.0	730.2	5.91

Notes. In the second column we list the masses of the companions including that of the PLF as it was a point source. In the third column we list the separations for the companions and the inner and outer disk. In the fourth column we list the most probable periods (for the disk part we assume a Keplerian motion). Finally, in the fifth c-olumn we list the ratio between the period of the companion or disk and the period of PDS 70 b to evidence possible orbital resonance.

Table 5. Mass estimation for PDS 70 c obtained from the SPHERE photometry and from the AMES-DUSTY models.

Spectral band	Mass ($M_{\rm Jup}$)
J	4.35 ± 0.45
H	4.21 ± 0.78
K1	4.31 ± 0.45
K2	4.02 ± 0.41

magnitudes are due to the planetary atmosphere and that the age of the companion is the same as the age of the star.

We also used the extracted photometry to build two color-magnitude diagrams. These were created following the procedure described in Bonnefoy et al. (2018) and are displayed in the left (J–H versus J) and right (J–K1 versus J) panels of Fig. 6. The positions of PDS 70 c in these two diagrams demonstrate that it is an extremely red object even with respect to PDS 70 b, which is also shown for comparison. The larger redness of PDS 70 c is also confirmed by the comparison of the spectra of these two objects in panel a of Fig. 5 where the K-band values for PDS 70 b are lower than those for PDS 70 c when the rescaling factor is taken into account. We overplot on both color-magnitude diagrams the reddening vectors due to interstellar extinction (Draine 2003) and those due to 0.5 μm forsterite grains using the optical constants by Scott & Duley (1996). These grains are proposed to explain the red colors of dusty and variable L dwarfs (Marocco et al. 2014; Bonnefoy et al. 2016). Both PDS 70 b and PDS 70 c appear to be shifted along these vectors with respect to the sequence of field dwarfs. These results are compatible with both these objects being low-mass objects strongly reddened by the presence of dust.

With the aim of characterizing this companion, we fitted its extracted spectrum with Exo-REM models taking into account the presence of thick clouds (Baudino et al. 2015, 2017; Charnay et al. 2018). The atmospheric models were calculated on a grid with $T_{\rm eff}$ varying between 300 and 2000 K with steps of 50 K and with $\log g$ with values between 3.0 and 6.0 dex with steps of 0.1 dex. On the other hand, we verified that the metallicity did not influence the final result, and assumed solar metallicity (we explored also the 0.3× and 3× solar metallicity). As can be seen in the panel a of Fig. 5, where the green solid line represents the best-fit Exo-REM model, the fit is good along all the extracted spectrum. Best fits are found for models with low gravity ($\log g \sim 3.0$–3.5) and for $T_{\rm eff}$ in the range 800–1100 K. The masses range between 0.5 and 4 $M_{\rm Jup}$ and are just partially in agreement with what we found previously with AMES-DUSTY models. The best-fit model represented in Fig. 5 has $T_{\rm eff} = 900$ K, $\log g = 3.1$ dex, $R = 1.95\ R_{\rm Jup}$ and $M = 1.93\ M_{\rm Jup}$.

To confirm these results we performed a similar procedure using the BT-Settl models (Allard 2014) with $T_{\rm eff}$ varying between 700 and 2500 K with a step of 100 K and a $\log g$ between 3.0 and 5.5 dex with a step of 0.5 dex. Also in this case we considered only solar metallicity. We obtained a good fit for $T_{\rm eff}$ between 800 and 1100 K and for $\log g = 3.5$. We can therefore conclude that the two models are in good agreement as also confirmed by the best-fit model displayed in Fig. 5 with the green dashed line. In this case the best fit is obtained for $T_{\rm eff} = 900$ K and $\log g = 3.5$ dex.

The recently suggested presence of a circumplanetary disk (Isella et al. 2019) may cause selective absorption, reddening the object spectrum. This would at least partially explain the very red colors that we found in our analysis and would confirm recent results on the detectability of circumplanetary disks from hydrodynamic simulation (Szulágyi & Garufi 2019; Szulágyi et al. 2019). The effects of the circumplanetary disk should be carefully modeled because they could partially modify the fitting results that we have found in this section, but this analysis is beyond the scope of the present work. The results presented here should be regarded as a first estimation of the physical characteristics of the companion.

4.2. The nature of the PLF

The fact that the PLF is recoverable in at least four different epochs is clear evidence that it is a real astrophysical signal. Moreover, its astrometric positions in the four epochs clearly exclude the possibility that it is a background object and they are in agreement with a Keplerian circular motion around the star. However, as discussed above, its spectrum is blue and very similar to the stellar spectrum. To confirm the reliability of the extracted spectrum we extracted the spectrum of a simulated planet with a spectrum and position similar to that of the PLF following the same method used for PDS 70 c and described in Sect. 4.1. The results are displayed in panel d of Fig. 5 where the input spectrum is represented by a black solid line while the extracted spectrum is represented by red circles. Like for the case of PDS 70 c, we are able to faithfully reproduce the input spectrum. A blue spectrum is a strong hint that the emission is due to stellar light reflected likely by dust. Its measured separation of ~13.5 au is not consistent with the radius of the inner disk of about 9 au (Keppler et al. 2019) corresponding to an angular radius of ~0.08″ that should be completely behind the SPHERE

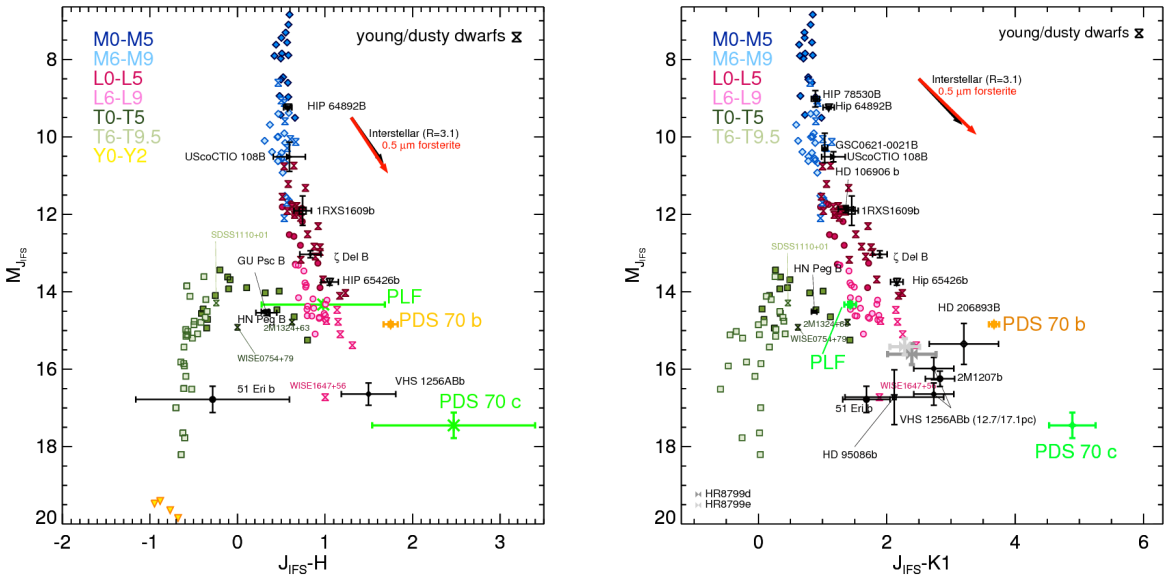

Fig. 6. *Left*: positions of PDS 70 c and of the PLF (green stars) in the J–H vs. J color-magnitude diagram. The position of PDS 70 b (orange star) is also indicated for comparison. We also display the positions of field dwarfs indicated with different symbols according to the spectral type and of some low-mass companions. Moreover, we overplot the reddening vector computed for the synthetic extinction curve using $R_V = 3.1$ (black arrow) and the reddening vector due to the extinction curve of forsterite (red arrow). *Right*: same as left panel but for the J–K1 versus J diagram.

coronagraph. We should however consider that the inner disk size is obtained in the submillimeter continuum that probes the distribution of large dust grains. We cannot exclude that the distribution of small dust grains, probed by scattered light, could be different.

A hint favoring this latter view comes from the analysis of the IFS off-axis PSF images obtained immediately before and after the coronagraphic observations as explained in Sect. 2. Exploiting the field rotation between these two images we can perform a subtraction to eliminate static speckles. This procedure is performed separately in Y, J, and H band. In normal conditions, the limiting contrast that we can obtain in the region between 60 and 110 mas from the star is of the order of 6–7 magnitudes. However, the very good conditions obtained during the night of 2018-02-24 allowed us to reach a contrast of the order of 10 magnitudes at the same separations. In Fig. 7 we present the results of this procedure on the H-band data. In this image there is a possible detection of the inner ring of the disk. We draw an ellipse (red solid line) adopting the inclination and the PA of 49.7° and 158.6°, respectively. Moreover, its semi-major axis is of 128 mas. This ellipse is roughly passing through the position of the PLF. While this is a differential image, it is not an ADI image because it uses only two frames. For this reason, we expect that the region on the near side of the disk around the semi-minor axis (corresponding to the forward scattering of the disk) is the brightest, as indeed it is. The contrast value in the position of the PLF is about 9.5 mag, consistent with the photometry obtained on the coronagraphic image. These results therefore appear consistent with scattered light from the inner disk. In any case, it is important to stress that while these results are suggestive of the presence of the inner disk, they cannot be considered as a clear detection due to the very low S/N of the signal and to the presence of other faint structures in the FOV. However, we would like to note that this structure has the expected orientation for the inner disk and that a comparison with other observations taken in similar optimal conditions as those for PDS 70 does not reveal similar structures. If the interpretation of this image as the inner disk is correct, then the PLF is a part of the disk itself.

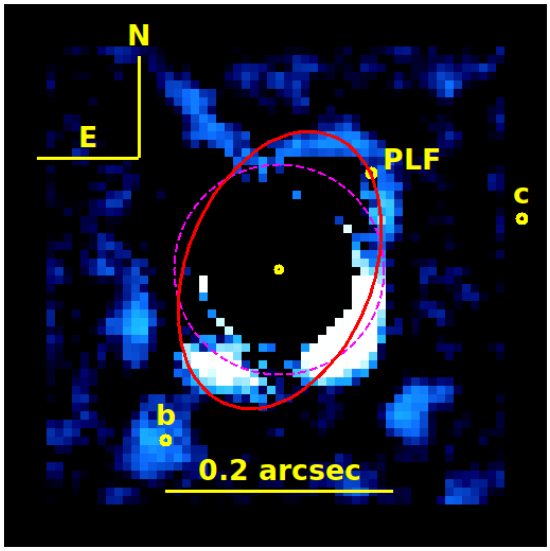

Fig. 7. Image resulting from the off-axis PSF subtraction described in the text. The red ellipse represents the estimated position for the inner disk. The dashed magenta circle represents the position of the coronagraph. The yellow circles are used to tag the positions of the point sources.

The positions of the PLF in both the color-magnitude diagrams displayed in Fig. 6 are compatible with those of field dwarfs with spectral type L6-L9. Moreover, we followed the same procedure used for PDS 70 c fitting its extracted spectrum both with Exo-REM and BT-Settl atmospheric models. The best-fit spectra from this procedure are shown in panel b of Fig. 5. Exo-REM models point toward a small star with a mass of ~100 $M_{\rm Jup}$ and $T_{\rm eff}$ between 1400 and 2000 K. The value of $\log g$ should be of the order of 6. On the other hand, BT-Settl models favor a much higher $T_{\rm eff}$ of the order of 3000 K while the surface gravity is unconstrained. These results are generally quite inconsistent with each other. Moreover, a small star at such

a short separation from the star would probably have a strong effect on the stability of the system generating a strong radial velocity signal that has never been observed. Furthermore, a stellar object would be much brighter than what we found for the PLF, by approximately 6–9 magnitudes. These considerations seem to confirm our previous conclusions that we are not actually looking to the photosphere of a sub-stellar object but rather to stellar light reflected by dust. If so, the inconsistent results obtained when attempting to fit this spectrum with the atmospheric models are naturally explained.

The results above seem to demonstrate that the PLF is actually a part of the inner disk, which is supported by the fact that no H_α emission associated to the PLF has been detected so far. Still, we cannot completely exclude the possibility that it is actually a point source that should be however embedded into the disk. If this were the case, we could consider two alternative possibilities. The first one is that the point source is a transient blob of dust that is destined to break apart over a timescale of few thousand years similar to blobs B and C seen in the disk of HD 169142 (Ligi et al. 2018; Gratton et al. 2019) and, for this reason, the probability to observe such a transient phenomenon is generally low unless these structures are generated frequently. The second possibility is that we are observing a dust envelope around a forming planet. This case would be very similar to what was suggested for blob D around HD 169142 with SPHERE data (Gratton et al. 2019). Given the spectrum, we should not see any photospheric emission from the planet due to the fact that the envelope is optically thick or the light reflected by the dust dominates over the photospheric emission. If this is the case, we can estimate the mass of the planet considering its contrast and assuming that the dust is filling the Hill radius around the planet. The contrast of the object is given by:

$$C = A \cdot \frac{\pi r_{\rm H}^2}{4\pi a^2} \cdot \frac{1}{k}, \tag{1}$$

where A is the albedo, $r_{\rm H}$ is the Hill radius, a is the separation of the object from the star and k is a multiplicative factor depending on the geometry of the system. Considering the inclination of the system, we found that a reasonable value of k is 1.38. The Hill radius is given by:

$$r_{\rm H} = a \cdot \sqrt[3]{\frac{m_{\rm p}}{3M_\star}}, \tag{2}$$

where $m_{\rm p}$ is the mass of the planet and $M_\star$ is the stellar mass. Joining Eqs. (1) and (2) we obtain an expression for the planetary mass:

$$m_{\rm p} = 3M_\star \cdot \left(\frac{4Ck}{A}\right)^{\frac{3}{2}}. \tag{3}$$

The value of the contrast is 7.27×10^{-5} as obtained from a median of the contrast values on each IFS spectral channel. We then assume for the star a mass of 0.76 $M_\odot$ (Müller et al. 2018) and an albedo (A) of 0.5, and obtain a value for the mass of the planet of 5.2×10^{-5} $M_\odot$ corresponding to ~17.3 $M_\oplus$. This is of course a lower limit, valid in the case where the circumplanetary material is filling the Hill radius. In a more evolved case, in which the circumplanetary material is filling one-third of the Hill radius as proposed for example by Ayliffe & Bate (2009) the mass of the planetary objects would be of the order of 90 $M_\oplus$. It this were true, in the PDS 70 system we would have planets at different evolution stages. Indeed, while PDS 70 b and PDS 70 c are accreting material probably from a circumplanetary disk, this object would still be in its formation phase. This would resemble the history of our Solar System where the gaseous giant planets formed before the inner planets.

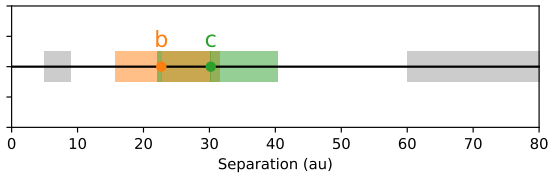

Fig. 8. Positions of the chaotic zones for PDS 70 b and PDS 70 c. The gray zones represent the disk positions.

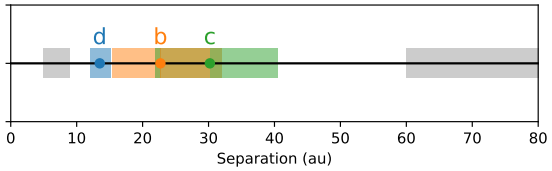

Fig. 9. Same as Fig. 8 but including also the PLF (here tagged as d) considering it as a real companion.

4.3. Stability of the system

To test the stability of the system, we performed a few N-body simulations with the integrator Swift HJS (Beust 2003). This method is optimized to check what happens in the disk cavity because it does not take into account the gas component of the disk. The main assumption of this model is that there is no major influence of the circumstellar disk on the planetary orbits. The critical parameters that control the stability of the system are the semi-major axes ratios and the eccentricities. To this aim we used the values listed in Table 4 for PDS 70 b and PDS 70 c. Given the current observational constraints, the stability of the system is not guaranteed if the masses are as large as obtained assuming an age of 5.4 Myr for the planets. The companions are not sufficiently separated to avoid significant gravitational interactions that would act within a timescale of the order of few thousand years, which is not compatible with the age of the system. The chaotic zones around each one of them can be computed from Morrison & Malhotra (2015). The case of coplanar circular orbits at the observed separations is represented in Fig. 8. The separation of PDS 70 c falls within the chaotic zone of PDS 70 b, indicating strong dynamical perturbations. If we assume that the PLF is actually a massive body with the mass determined in Sect. 4.2 the results on the stability do not change due to its proposed low mass. As shown in Fig. 9, it is outside the chaotic zones of its neighbor, but not by far, meaning that eccentricity fluctuations could eventually destabilize it. Assuming circular orbits for all three companions in order to limit dynamical perturbations still leads to a destabilization within a few thousand years. Given the age of the system, this is not likely to be the case. The companion separations are compatible with a configuration of mean-motion resonances 1:2:3, and marginally with a 1:2:4 configuration. This system would therefore be very similar to the four-planet system HR 8799 (Marois et al. 2008), which also appeared unstable and is potentially in a resonant configuration (Goździewski & Migaszewski 2009) or stable on the condition that the planets are coplanar or in mean-motion resonance (Konopacky et al. 2016; Wang et al. 2018). A comprehensive study of the dynamics of PDS 70 would need to take into account both the mean-motion resonances and the interactions with the disk, which could act as

a stabilizing factor by damping the eccentricities. On the other hand, to first order, both the inner disk and outer disk edges are compatible with the positions of the bodies. Furthermore, the disk is susceptible to be affected by the gravitational influence of the PLF (if this is real) for the inner disk and PDS 70 c for the outer disk, through secular dynamics and mean-motion resonances. This could cause local depletions in some part of the disk or asymmetries. However, to study in more detail these effects we would need hydrodynamical simulations of the disk evolution and this is outside the scope of this paper.

We would like to stress that these results have been achieved assuming masses for PDS 70 b and PDS 70 c obtained using the system age of 5.4 Myr. Anyhow, given that these two objects are still in formation, their ages could be younger and as a consequence their masses would also be lower changing the results concerning the stability of the system. Indeed, stability simulations performed with lower masses for PDS 70 b and PDS 70 c (2 $M_{\rm Jup}$) would allow stability to be reached also when we change only the mass of one of the two planets if the separation of PDS 70 c is 31 au or larger. The orbital parameters of this object were determined thanks to only two astrometric points; further astrometric measurements will be needed to better constrain them. If we were to instead consider the two masses given in Table 4 for these two objects, we would need a separation larger than 35–36 au for PDS 70 c or alternatively a separation smaller than 20 au for PDS 70 b, indeed only in the case where the PLF is not a companion.

The system stability could be enhanced if the two planets are in mean-motion resonance as found recently by Bae et al. (2019) using two-dimensional hydrodynamic simulations.

5. Conclusions

Here, we present SPHERE observations aiming to verify the presence of a second planetary companion around the star PDS 70. Our results confirm the presence of PDS 70 c both in J- and H-spectral bands with IFS and in K band with IRDIS despite the flux being very low at shorter wavelengths. We retrieved astrometric positions for this object at two different epochs and this allowed us to show that this object is actually gravitationally bound to the star. The extracted photometry hints toward a very red spectrum that is very probably due to the presence of dust in the planetary atmosphere and/or to the presence of a circumplanetary disk as proposed through recent ALMA observations. We were able to obtain a good fit with atmospheric models and our results clearly tend toward a low-gravity (3.0–3.5 dex) and low-temperature (∼900 K) object using both the Exo-REM and the BT-Settl models. The mass evaluated through these models is in marginal agreement with that obtained through the AMES-DUSTY evolutionary models, but we can however conclude that it should be less than ∼5 $M_{\rm Jup}$. Finally, the probable presence of dust in the atmosphere of this object and/or of a circumplanetary disk is also confirmed by its position in the color-magnitude diagram, which is even more extreme than that of PDS 70 b.

In addition to the results on PDS 70 c, the analysis of archival and new data allowed us to detect the presence of a possible third point source in this planetary system (PLF). This object is located at small separation (∼0.12″) from the star and is clearly detected only in the IFS data while it is barely visible in the IRDIS data. In any case, it was possible to detect it at four different epochs with a time range of about three years allowing us to exclude the idea that it is simply a feature due to the speckle subtraction method. Also, these astrometric positions allowed us to confirm that this object is actually gravitationally bound to the star. However, the extracted spectrum for this object is blue hinting toward stellar light reflected from dust. This result seems to demonstrate that this object is actually a feature due to the inner disk. This is further confirmed by an analysis of the non-coronagraphic PSF data from which we were able to find hints of the presence of the inner disk at the separation of this feature. We cannot however definitely exclude the possibility that it is a separate object, and in this case we considered two possible solutions. The first one is that it is simply a transient blob of dust while in the second solution it could be a forming planet completely embedded in a dust envelope. Inline with the first solution we should assume that the generation of such blobs is frequent through some poorly defined mechanism. If the second solution was accurate we would not be able to see any light from the planetary photosphere and this would justify the extracted spectrum. If this latter scenario represents the real nature of this object we can evaluate its mass being less than 90 $M_{\oplus}$. It is not possible with the present data to draw a definitive conclusion about the nature of this object. Interferometric data for the inner part of this system taken with an instrument such as GRAVITY (Gravity Collaboration 2017) for example would be needed to be able to obtain a definitive answer on this point.

We also present a possible solution for the general structure of the planetary system assuming circular orbits for all the candidate companions. Moreover, the simulations were performed both excluding and including the PLF. In both cases, the proposed configuration does not seem to be stable on long periods if the masses are as large as obtained assuming that the age of the companions is the same as for the star. In any case, as noted above, lower masses of the companions due to a lower age of the forming planets with respect to the system would allow us to obtain a stable configuration. Clearly, long-period astrometric follow-up observations will be needed to further constrain the orbits of the proposed objects and to draw more precise conclusions about the structure and the stability of the PDS 70 system.

From our data we can conclude that PDS 70 hosts the second multiple planetary system found with the direct imaging technique and the first one at a very young age, where the planets are still accreting.

Acknowledgements. The authors thanks the anonymous referee for the constructive comments that strongly helped to improve the quality of this work. This work has made use of the SPHERE Data Center, jointly operated by OSUG/IPAG (Grenoble), PYTHEAS/LAM/CeSAM (Marseille), OCA/Lagrange (Nice) and Observatoire de Paris/LESIA (Paris). This work has made use of data from the European Space Agency (ESA) mission *Gaia* (https://www.cosmos.esa.int/gaia), processed by the *Gaia* Data Processing and Analysis Consortium (DPAC, https://www.cosmos.esa.int/web/gaia/dpac/consortium). Funding for the DPAC has been provided by national institutions, in particular the institutions participating in the *Gaia* Multilateral Agreement. This research has made use of the SIMBAD database, operated at CDS, Strasbourg, France. D.M., R.G., S.D., and A.Z. acknowledge support from the "Progetti Premiali" funding scheme of the Italian Ministry of Education, University, and Research. A.Z. acknowledges support from the CONICYT + PAI/Convocatoria nacional subvención a la instalación en la academia, convocatoria 2017 + Folio PAI77170087. A.M. acknowledges the support of the DFG priority program SPP 1992 "Exploring the Diversity of Extrasolar Planets" (MU 4172/1-1). C.P. acknowledge financial support from Fondecyt (grant 3190691) and financial support from the ICM (Iniciativa Científica Milenio) via the Núcleo Milenio de Formación Planetaria grant, from the Universidad de Valparaíso. T.H. acknowledges support from the European Research Council under the Horizon 2020 Framework Program via the ERC Advanced Grant Origins 83 24 28. SPHERE is an instrument designed and built by a consortium consisting of IPAG (Grenoble, France), MPIA (Heidelberg, Germany), LAM (Marseille, France), LESIA (Paris, France), Laboratoire Lagrange (Nice, France), INAF-Osservatorio di Padova (Italy), Observatoire de Genève (Switzerland), ETH Zurich (Switzerland), NOVA (Netherlands), ONERA (France) and ASTRON

(Netherlands), in collaboration with ESO. SPHERE was funded by ESO, with additional contributions from CNRS (France), MPIA (Germany), INAF (Italy), FINES (Switzerland) and NOVA (Netherlands). SPHERE also received funding from the European Commission Sixth and Seventh Framework Programmes as part of the Optical Infrared Coordination Network for Astronomy (OPTICON) under grant number RII3-Ct-2004-001566 for FP6 (2004-2008), grant number 226604 for FP7 (2009-2012) and grant number 312430 for FP7 (2013-2016).

References

Allard, F. 2014, IAU Symp., 299, 271
Allard, F., Hauschildt, P. H., Alexander, D. R., Tamanai, A., & Schweitzer, A. 2001, ApJ, 556, 357
Asensio-Torres, R., Currie, T., Janson, M., et al. 2019, A&A, 622, A42
Ayliffe, B. A., & Bate, M. R. 2009, MNRAS, 397, 657
Bae, J., Zhu, Z., Baruteau, C., et al. 2019, ApJ, 884, L41
Baudino, J. L., Bézard, B., Boccaletti, A., et al. 2015, A&A, 582, A83
Baudino, J. L., Bonnefoy, M., Vigan, A., & Irwin, P. J. 2017, in SF2A-2017: Proceedings of the Annual meeting of the French Society of Astronomy and Astrophysics, eds. C. Reylé, P. Di Matteo, F. Herpin, et al., 343
Beust, H. 2003, A&A, 400, 1129
Beuzit, J.-L., Vigan, A., Mouillet, D., et al. 2019, A&A, 631, A155
Binnendijk, L. 1960, Properties of Double Stars; a Survey of Parallaxes and Orbits (Whitefish, USA: Literary Licensing)
Bonnefoy, M., Lagrange, A. M., Boccaletti, A., et al. 2011, A&A, 528, L15
Bonnefoy, M., Zurlo, A., Baudino, J. L., et al. 2016, A&A, 587, A58
Bonnefoy, M., Perraut, K., Lagrange, A. M., et al. 2018, A&A, 618, A63
Cantalloube, F., Mouillet, D., Mugnier, L. M., et al. 2015, A&A, 582, A89
Charnay, B., Bézard, B., Baudino, J. L., et al. 2018, ApJ, 854, 172
Chauvin, G., Desidera, S., Lagrange, A. M., et al. 2017, in SF2A-2017: Proceedings of the Annual meeting of the French Society of Astronomy and Astrophysics, eds. C. Reylé, P. Di Matteo, F. Herpin, et al., 331
Christiaens, V., Cantalloube, F., Casassus, S., et al. 2019a, ApJ, 877, L33
Christiaens, V., Casassus, S., Absil, O., et al. 2019b, MNRAS, 486, 5819
Claudi, R. U., Turatto, M., Gratton, R. G., et al. 2008, SPIE Conf. Ser., 7014, 70141Z
de Boer, J., Salter, G., Benisty, M., et al. 2016, A&A, 595, A114
Delorme, P., Meunier, N., Albert, D., et al. 2017, in SF2A-2017: Proceedings of the Annual meeting of the French Society of Astronomy and Astrophysics, eds. C. Reylé, P. Di Matteo, F. Herpin, et al., 347
Desidera, S., Carolo, E., Gratton, R., et al. 2011, A&A, 533, A90
Dohlen, K., Langlois, M., Saisse, M., et al. 2008, SPIE Conf. Ser., 7014, 3
Dong, R., Hashimoto, J., Rafikov, R., et al. 2012, ApJ, 760, 111
Draine, B. T. 2003, ARA&A, 41, 241
Flasseur, O., Denis, L., Thiébaut, É., & Langlois, M. 2018, A&A, 618, A138
Gaia Collaboration (Brown, A. G. A., et al.) 2016, A&A, 595, A2
Gaia Collaboration (Brown, A. G. A., et al.) 2018, A&A, 616, A1
Galicher, R., Boccaletti, A., Mesa, D., et al. 2018, A&A, 615, A92
Goździewski, K., & Migaszewski, C. 2009, MNRAS, 397, L16
Gratton, R., Ligi, R., Sissa, E., et al. 2019, A&A, 623, A140
Gravity Collaboration (Abuter, R., et al.) 2017, A&A, 602, A94
Haffert, S. Y., Bohn, A. J., de Boer, J., et al. 2019, Nat. Astron., 329
Hashimoto, J., Dong, R., Kudo, T., et al. 2012, ApJ, 758, L19
Hashimoto, J., Tsukagoshi, T., Brown, J. M., et al. 2015, ApJ, 799 , 43
Heintz, W. 2000, Encyclopedia of Astronomy and Astrophysics, ed. P. Murdin, (Bristol: Institute of Physics Publishing), 2855
Isella, A., Benisty, M., Teague, R., et al. 2019, ApJ, 879, L25
Keppler, M., Benisty, M., Müller, A., et al. 2018, A&A, 617, A44
Keppler, M., Teague, R., Bae, J., et al. 2019, A&A, 625, A118
Konopacky, Q. M., Marois, C., Macintosh, B. A., et al. 2016, AJ, 152, 28
Ligi, R., Vigan, A., Gratton, R., et al. 2018, MNRAS, 473, 1774
Long, Z. C., Akiyama, E., Sitko, M., et al. 2018, ApJ, 858, 112
Marocco, F., Day-Jones, A. C., Lucas, P. W., et al. 2014, MNRAS, 439, 372
Marois, C., Macintosh, B., Barman, T., et al. 2008, Science, 322, 1348
Marois, C., Correia, C., Galicher, R., et al. 2014, Proc. SPIE, 9148, 91480U
Mesa, D., Gratton, R., Zurlo, A., et al. 2015, A&A, 576, A121
Metchev, S. A., Hillenbrand, L. A., & Meyer, M. R. 2004, ApJ, 600, 435
Morrison, S., & Malhotra, R. 2015, ApJ, 799, 41
Müller, A., Keppler, M., Henning, T., et al. 2018, A&A, 617, L2
Pavlov, A., Möller-Nilsson, O., Feldt, M., et al. 2008, SPIE Conf. Ser., 7019, 39
Pecaut, M. J., & Mamajek, E. E. 2016, MNRAS, 461, 794
Riaud, P., Mawet, D., Absil, O., et al. 2006, A&A, 458, 317
Scott, A., & Duley, W. W. 1996, ApJS, 105, 401
Sissa, E., Gratton, R., Garufi, A., et al. 2018, A&A, 619, A160
Soummer, R., Pueyo, L., & Larkin, J. 2012, ApJ, 755, L28
Szulágyi, J., & Garufi, A. 2019, ArXiv e-prints [arXiv:1906.01416]
Szulágyi, J., Dullemond, C. P., Pohl, A., & Quanz, S. P. 2019, MNRAS, 487, 1248
Vigan, A., Moutou, C., Langlois, M., et al. 2010, MNRAS, 407, 71
Wagner, K., Follete, K. B., Close, L. M., et al. 2018, ApJ, 863, L8
Wang, J. J., Graham, J. R., Dawson, R., et al. 2018, AJ, 156, 192
Zurlo, A., Vigan, A., Hagelberg, J., et al. 2013, A&A, 554, A21
Zurlo, A., Vigan, A., Mesa, D., et al. 2014, A&A, 572, A85
Zurlo, A., Mesa, D., Desidera, S., et al. 2018, MNRAS, 480, 35

[1] INAF – Osservatorio Astronomico di Padova, Vicolo dell'Osservatorio 5, 35122 Padova, Italy
e-mail: dino.mesa@inaf.it
[2] Max-Planck-Institut für Astronomie, Königstuhl 17, 69117 Heidelberg, Germany
[3] Univ. Grenoble Alpes, CNRS, IPAG, 38000 Grenoble, France
[4] LESIA, Observatoire de Paris, PSL Research University, CNRS, Sorbonne Univ., UPMC Univ. Paris 06, Univ. Paris Diderot, Sorbonne, Paris Cité, 5 Place Jules Janssen, 92195 Meudon, France
[5] Univ. Lyon, Univ. Lyon 1, ENS de Lyon, CNRS, CRAL UMR 5574, 69230 Saint-Genis-Laval, France
[6] Aix Marseille Univ., CNRS, CNES, LAM, Marseille, France
[7] Université de Lyon, UJM-Saint-Etienne, CNRS, Institut d'Optique Graduate School, Laboratoire Hubert Curien UMR 5516, 42023 Saint-Etienne, France
[8] Department of Terrestrial Magnetism, Carnegie Institution for Science, 5241 Broad Branch Road, NW, Washington, DC 20015, USA
[9] Unidad Mixta Internacional Franco-Chilena de Astronomía (CNRS, UMI 3386), Departamento de Astronomía, Universidad de Chile, Camino El Observatorio 1515, Las Condes, Santiago, Chile
[10] Leiden Observatory, Leiden University, PO Box 9513, 2300 RA Leiden, The Netherlands
[11] Department of Astronomy, University of Michigan, 1085 S. University Ave, Ann Arbor, MI 48109-1107, USA
[12] European Southern Observatory (ESO), Alonso de Cordova 3107, Vitacura, Casilla 19001, Santiago, Chile
[13] SPGroup, ELEN/ICTEAM, UCLouvain, 1348 Louvain-la-Neuve, Belgium
[14] Nucleo de Astronomia, Facultad de Ingenieria y Ciencias, Universidad Diego Portales, Av. Ejercito 441, Santiago, Chile
[15] Escuela de Ingenieria Industrial, Facultad de Ingenieria y Ciencias, Universidad Diego Portales, Av. Ejercito 441, Santiago, Chile
[16] INAF – Osservatorio Astronomico di Roma, via di Frascati 33, 00078 Monte Porzio Catone, Italy
[17] Department of Physics, University of Oxford, Oxford OX1 3PU, UK
[18] INAF – Osservatorio Astronomico di Capodimonte, Salita Moiariello 16, 80131 Napoli, Italy
[19] Geneva Observatory, University of Geneva, Chemin des Mailettes 51, 1290 Versoix, Switzerland
[20] Department of Astronomy, Stockholm University, Stockholm, Sweden
[21] Université Côte d'Azur, OCA, CNRS, Lagrange, France
[22] INAF – Osservatorio Astronomico di Brera, Via E. Bianchi 46, 23807 Merate, Italy
[23] STAR Institute, Université de Liège, Allée du Six Août 19c, 4000 Liège, Belgium
[24] Instituto de Física y Astronomía, Facultad de Ciencias, Universidad de Valparaíso, Av. Gran Bretaña 1111, Valparaíso, Chile
[25] Núcleo Milenio Formación Planetaria – NPF, Universidad de Valparaíso, Av. Gran Bretana 1111, Valparaíso, Chile
[26] Monash Centre for Astrophysics (MoCA) and School of Physics and Astronomy, Monash University, Clayton Vic 3800, Australia
[27] DOTA, ONERA, Univ. Paris Saclay, 91123, Palaiseau, France
[28] Hamburger Sternwarte, Gojenbergsweg 112, 21029 Hamburg, Germany